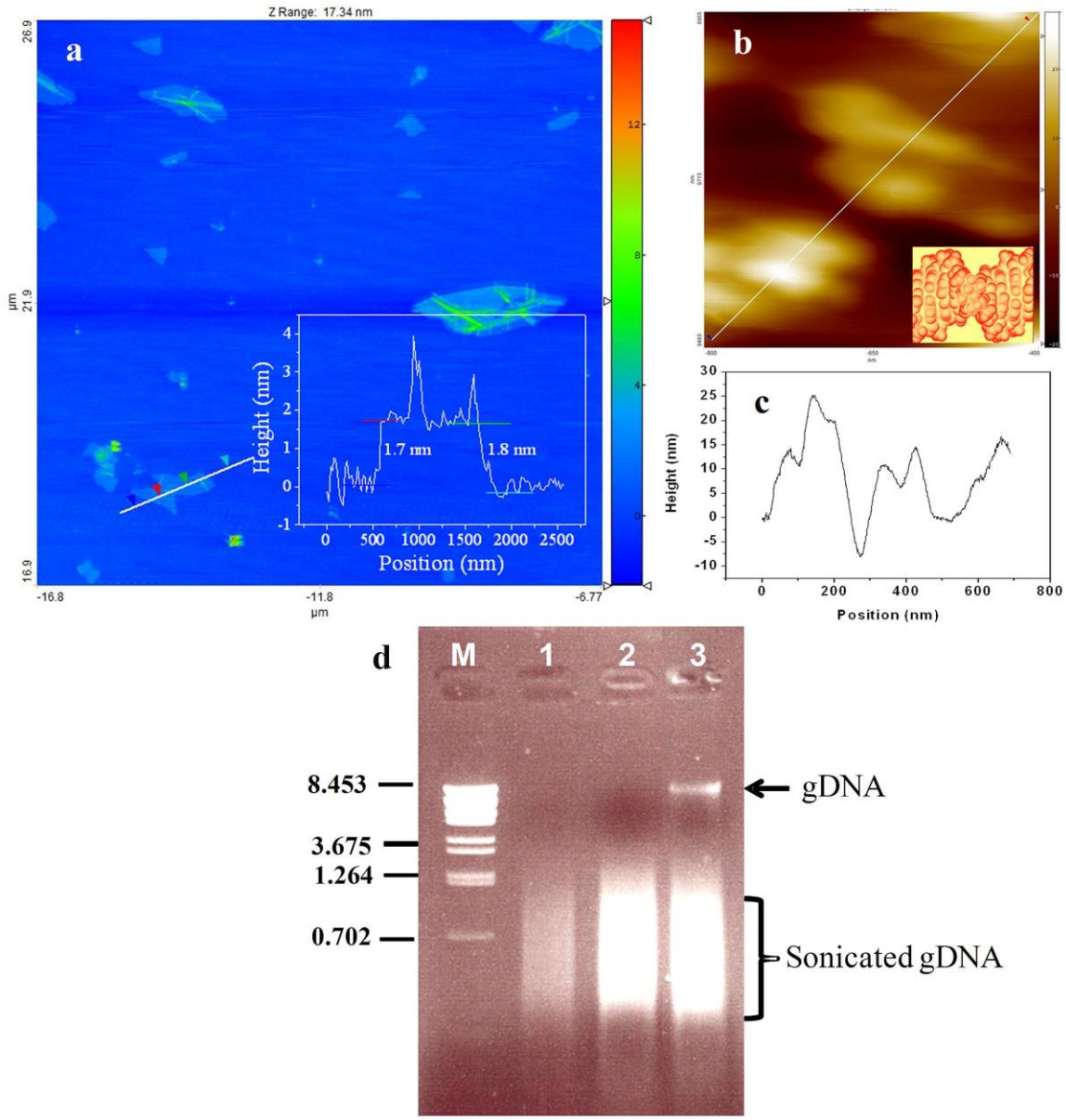

Supplementary Figure S1: AFM and gel electrophoresis images of GO and gDNA. (a) AFM image of GO and accompanying height profile (inset in Figure a). (b) AFM image of gDNA and related size profile (c). Inset of Figure S1(b) shows a simple representation of the gDNA structure. (d) Gel electrophoresis of gDNA isolated from *A. thaliana* plant leaves before and after sonication verified gDNA fragment size. Lanes: (M) size marker, (1) 500 and (2) 2500 ng sonicated gDNA, and (3) 750 ng unsonicated and 2500 ng sonicated gDNA.

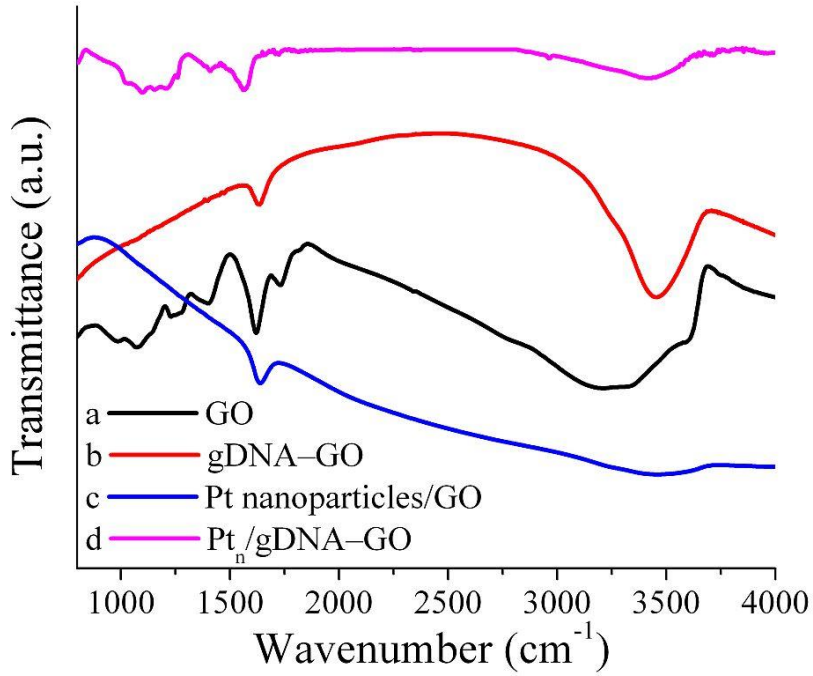

Supplementary Figure S2: FTIR analysis. FTIR spectra of (a) GO, (b) gDNA–GO, (c) Pt nanoparticles/GO and (d) Pt_n/gDNA–GO.

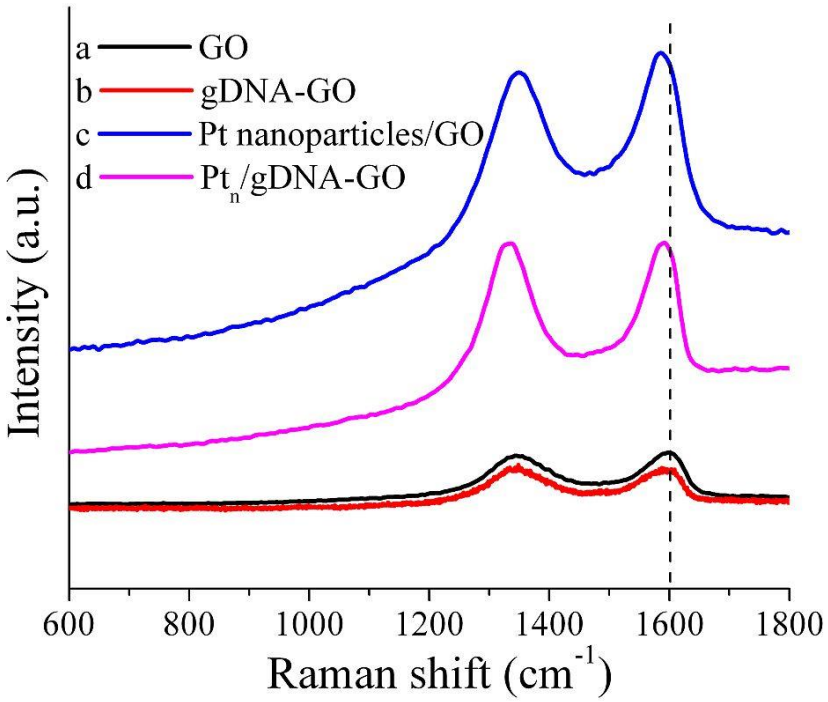

Supplementary Figure S3: Raman analysis. Raman spectra of (a) GO, (b) gDNA–GO, (c) Pt nanoparticles/GO and (d) Pt_n/gDNA–GO.

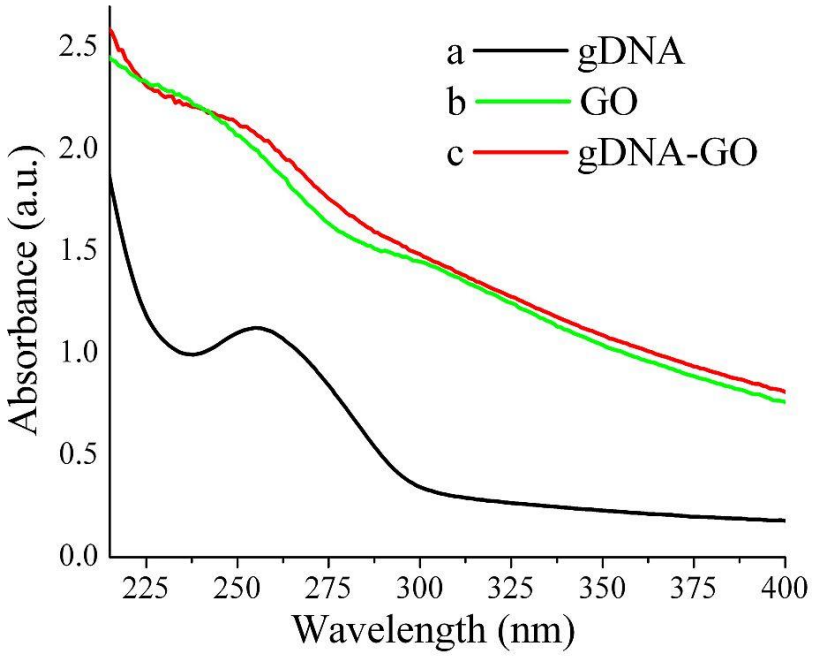

Supplementary Figure S4: UV–vis analysis. UV–vis absorption spectrum of (a) gDNA, (b) GO and (c) gDNA–GO in aqueous solution.

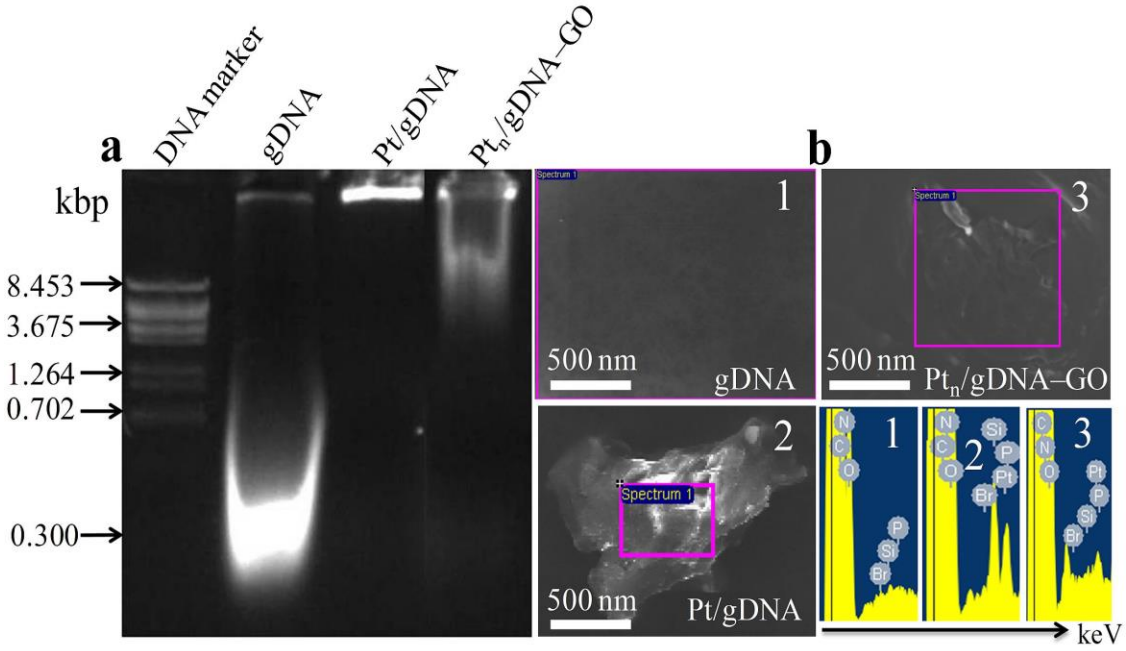

Supplementary Figure S5: Gel electrophoresis image and EDX analysis. (a) Gel electrophoresis of DNA size marker, gDNA, Pt/gDNA and Pt_n/gDNA-GO. Size of gDNA shown in kilo base pairs (kbp). (b) SEM images of gDNA, Pt/gDNA and Pt_n/gDNA-GO and their corresponding EDX analysis. For EDX analysis we cut the visible gDNA gel electrophoresis bands of the samples. In EDX analysis the Si peak appears due to the use of a Si wafer as a substrate. The observed Br peak is due to ethidium bromide which was used to detect the gDNA. The migration of the composite material in the electrophoresis gel is determined by its total negative charge. As the composite material is less negative than gDNA, due to bond formation between Pt^{2+} and the negatively charged DNA, it migrates a shorter distance in the gel than the gDNA.

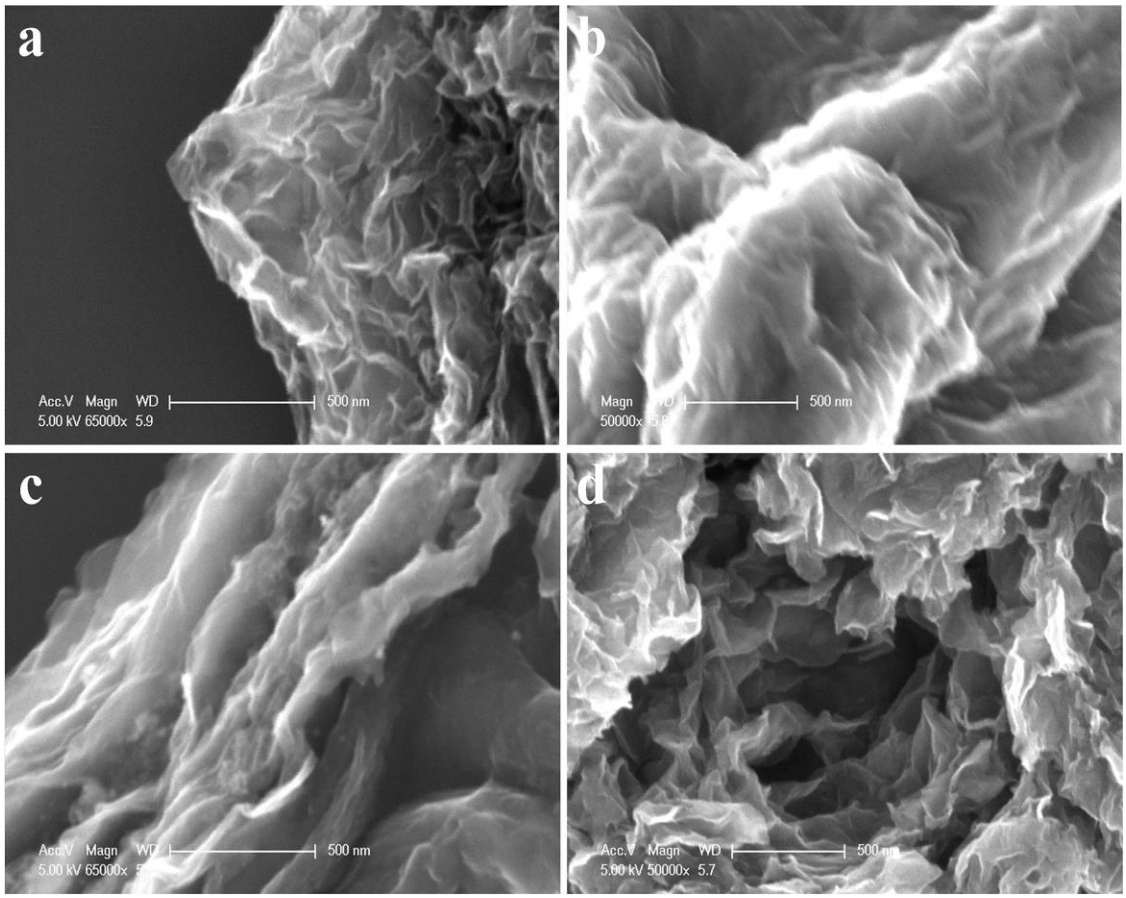

Supplementary Figure S6: Microstructure characterization. SEM images of (a) GO, (b) gDNA treated GO, (c) Pt nanoparticles/GO and (d) Pt_n/gDNA–GO composite.

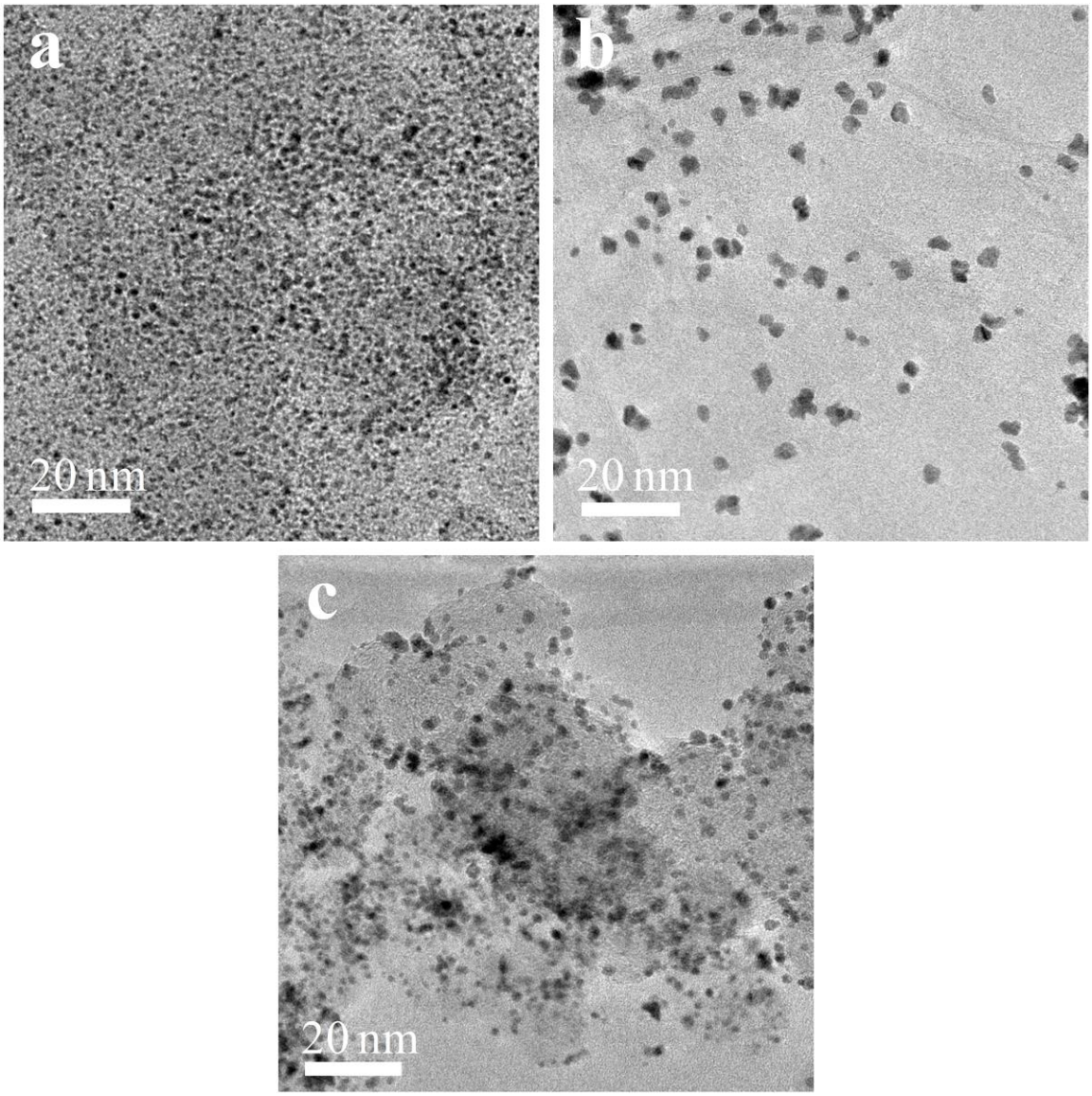

Supplementary Figure S7: Microstructure characterization. LRTEM images of gDNA treated GO, (a) Pt nanoparticles/GO, (b) Pt_n/gDNA–GO composite and (c) Pt/C catalyst.

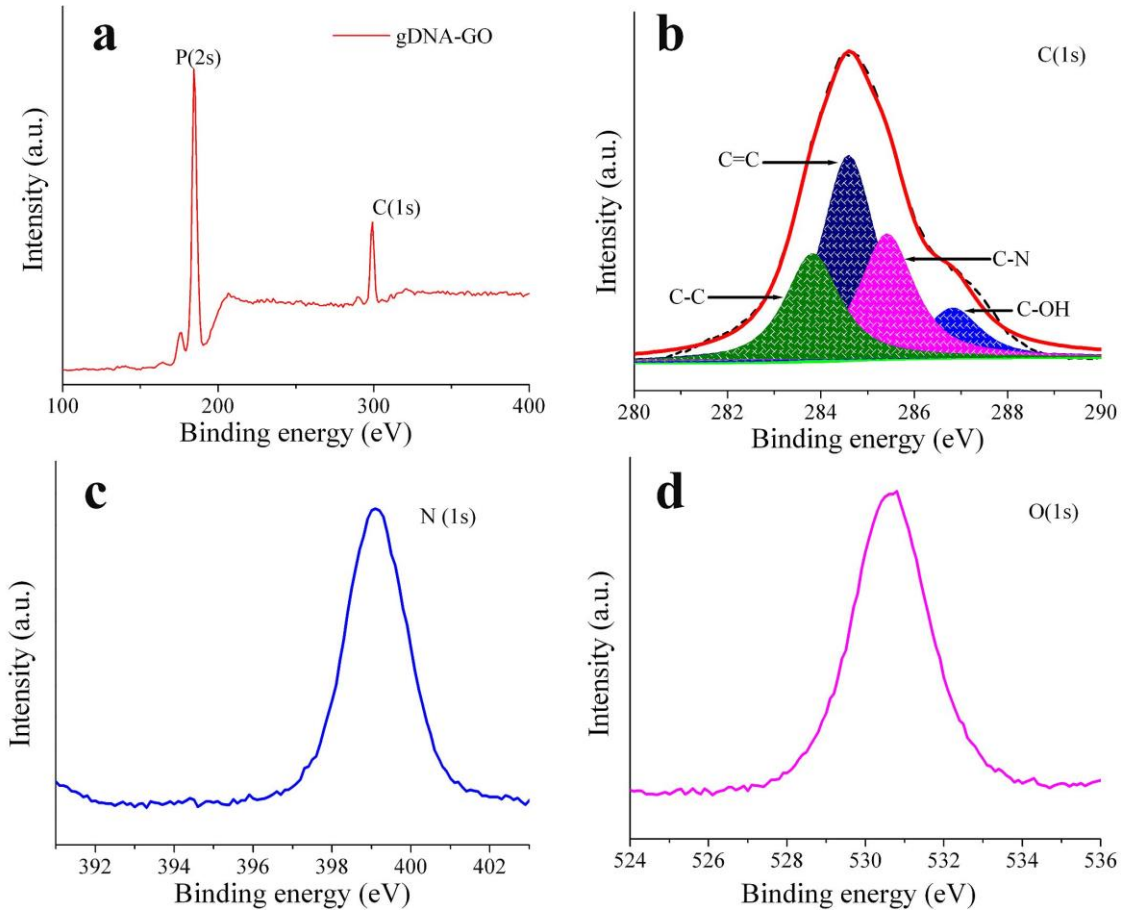

Supplementary Figure S8: XPS spectrum of the gDNA–GO composite. (a) Full survey spectra, (b) C1s core level spectrum, (c) N1s core level spectrum, and (d) O1s core level spectrum.

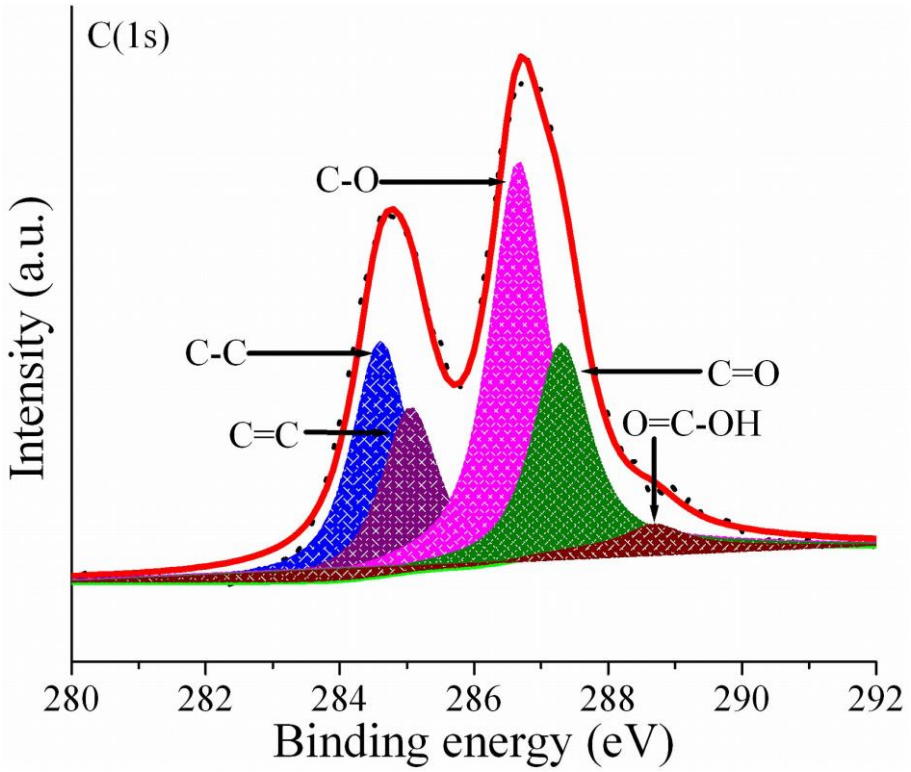

Supplementary Figure S9: XPS analysis of GO. XPS spectrum of the C1s core level of GO.

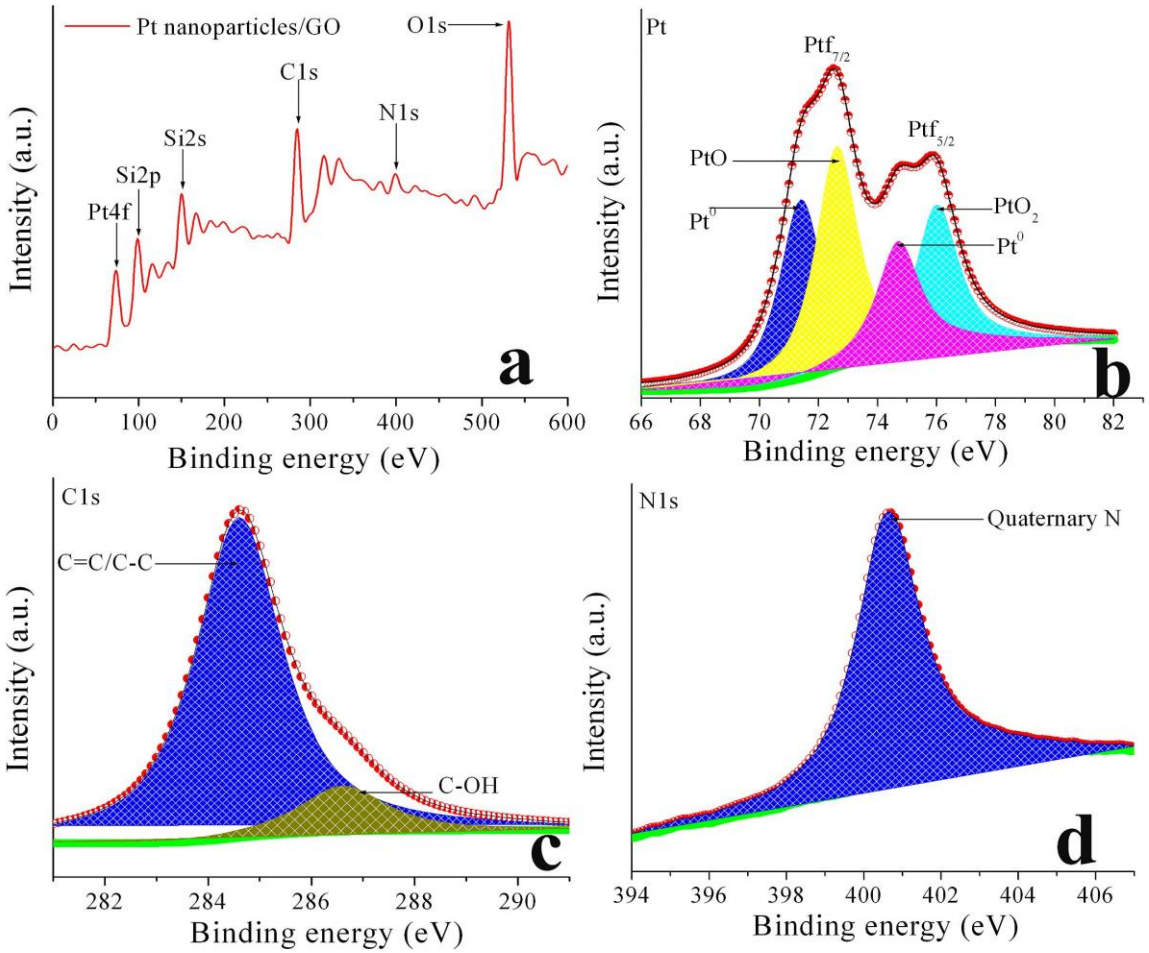

Supplementary Figure S10: XPS spectra of the Pt nanoparticles/GO composite. (a) full survey spectrum, (b) Pt core level spectrum, (c) C1s core level spectrum and (d) N1s core level spectrum.

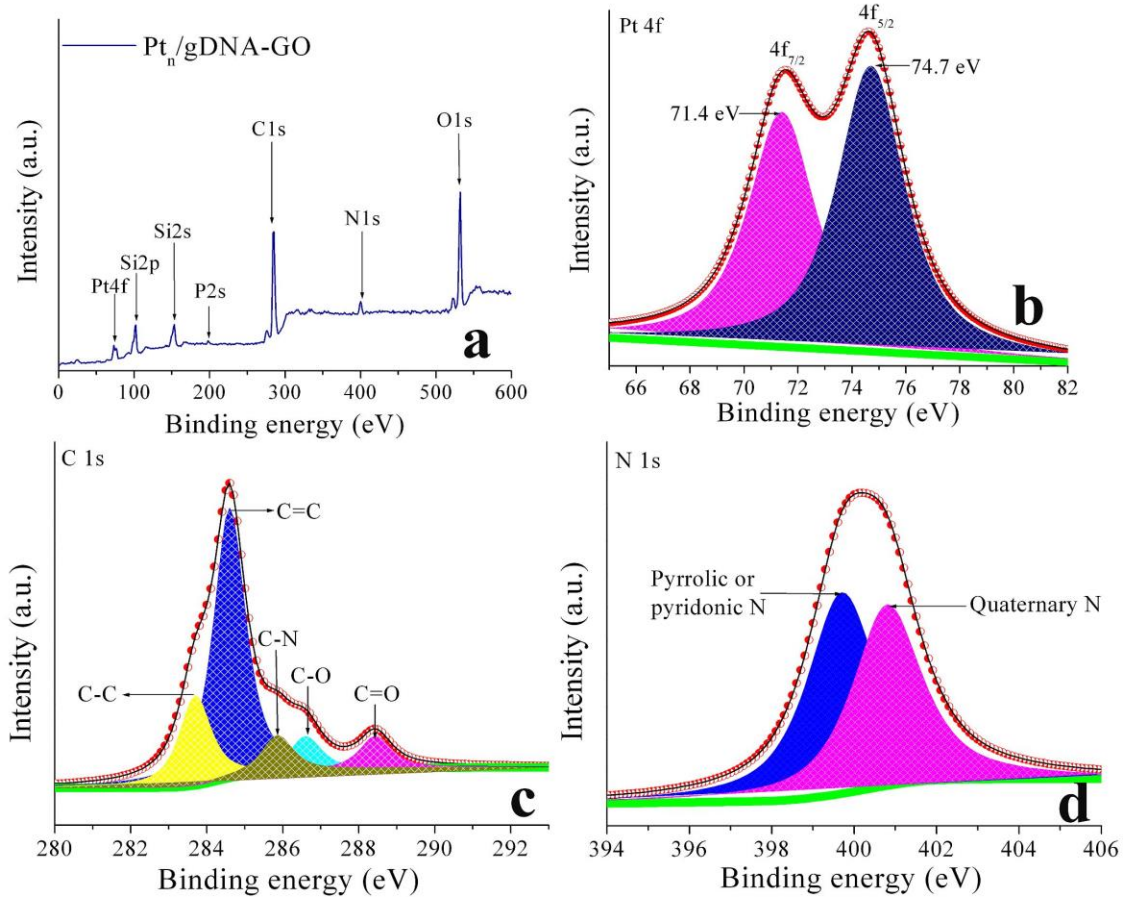

Supplementary Figure S11: XPS spectra of the Pt_n/gDNA–GO composite. (**a**) full survey spectra, (**b**) Pt core level spectra, (**c**) C1s core level spectra, and (**d**) N1s core level spectra.

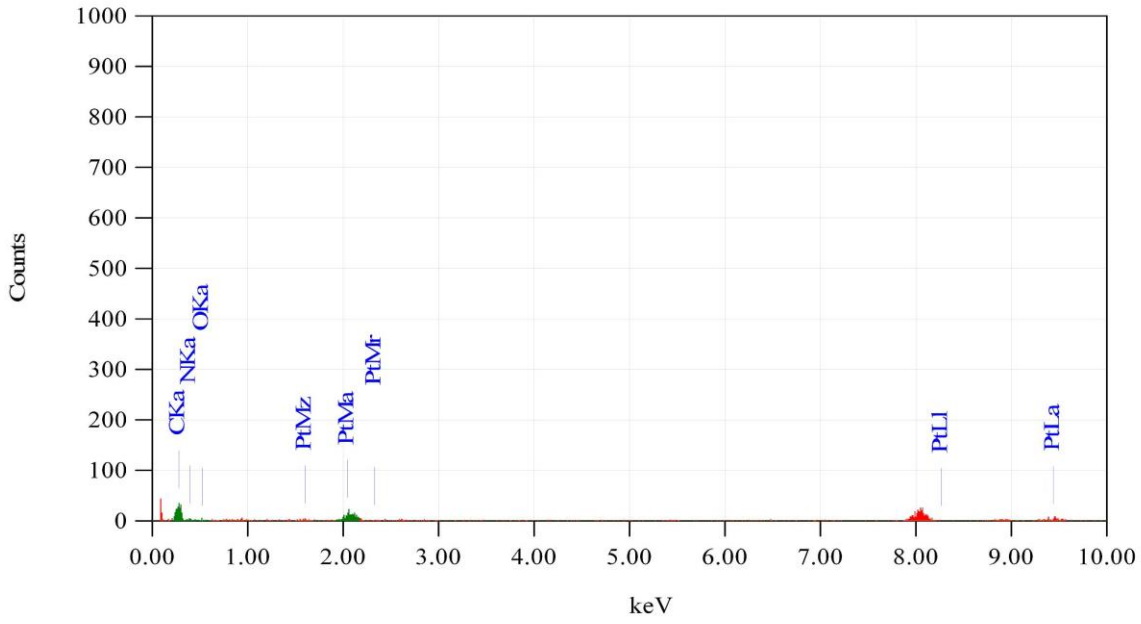

Supplementary Figure S12: EDX spectra. EDX pattern of the Pt_n/gDNA–GO composite.

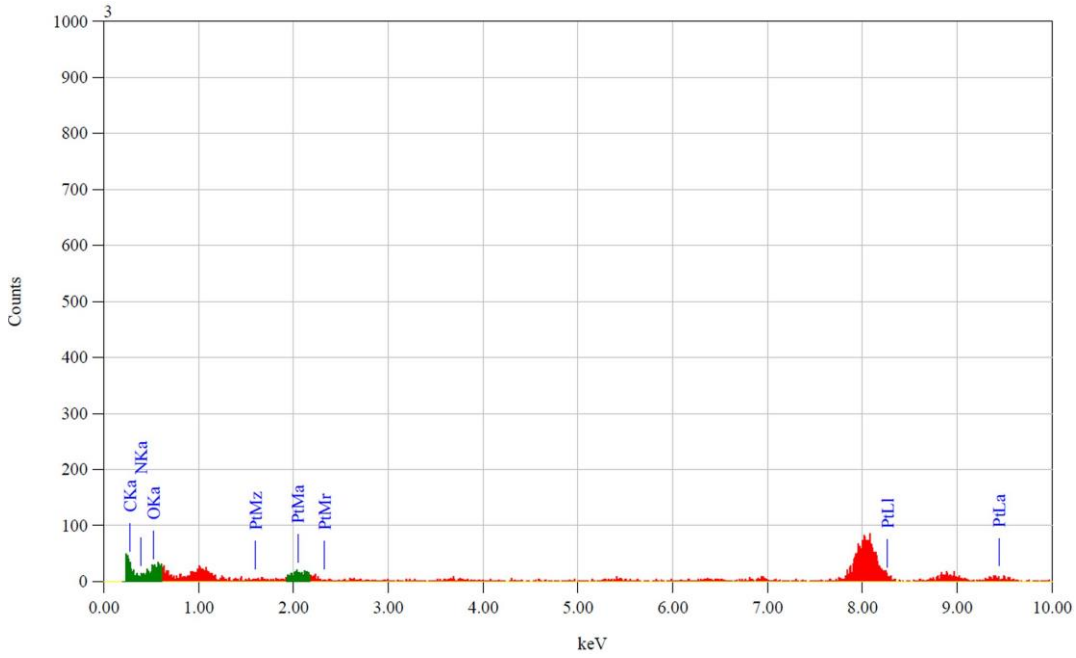

Supplementary Figure S13: EDX spectra. EDX pattern of the Pt nanoparticles/GO composite.

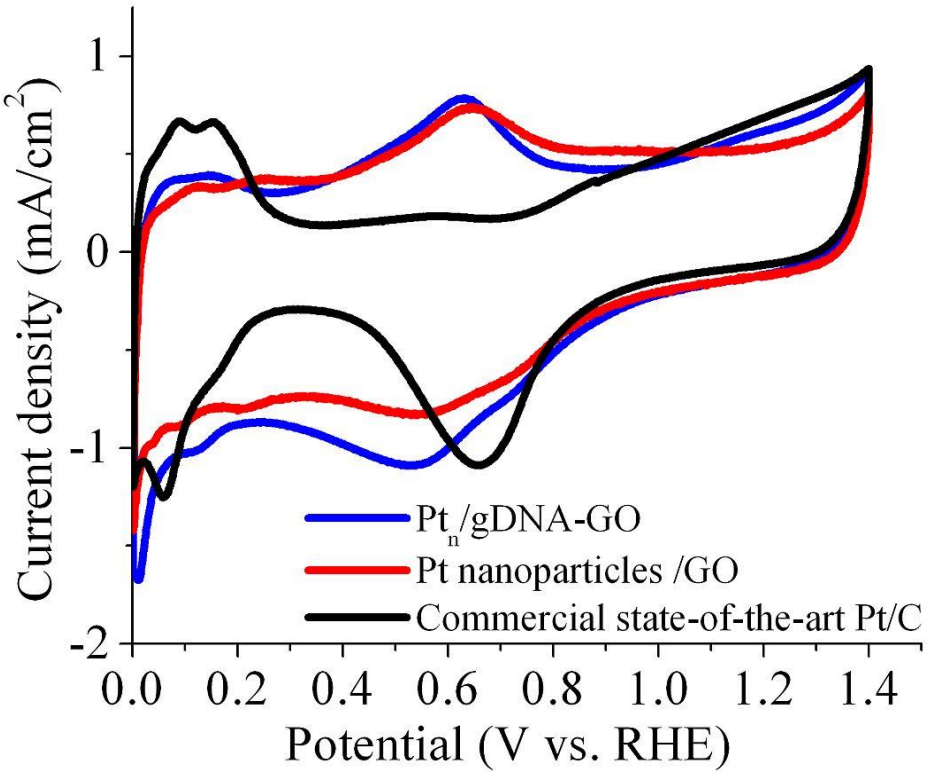

Supplementary Figure S14: Hydrogen adsorption/desorption CV scan. Comparison of the hydrogen adsorption/desorption voltammetric peaks at 50 mV/s in N_2-saturated 0.1 M $HClO_4$ for the three catalysts. The current density was normalized in reference to the geometric area of a rotating-disk electrode. The metal loading was ~11.3 µg/cm^2 on the GCE for the Pt_n/gDNA–GO, Pt nanoparticles/GO and Pt/C.

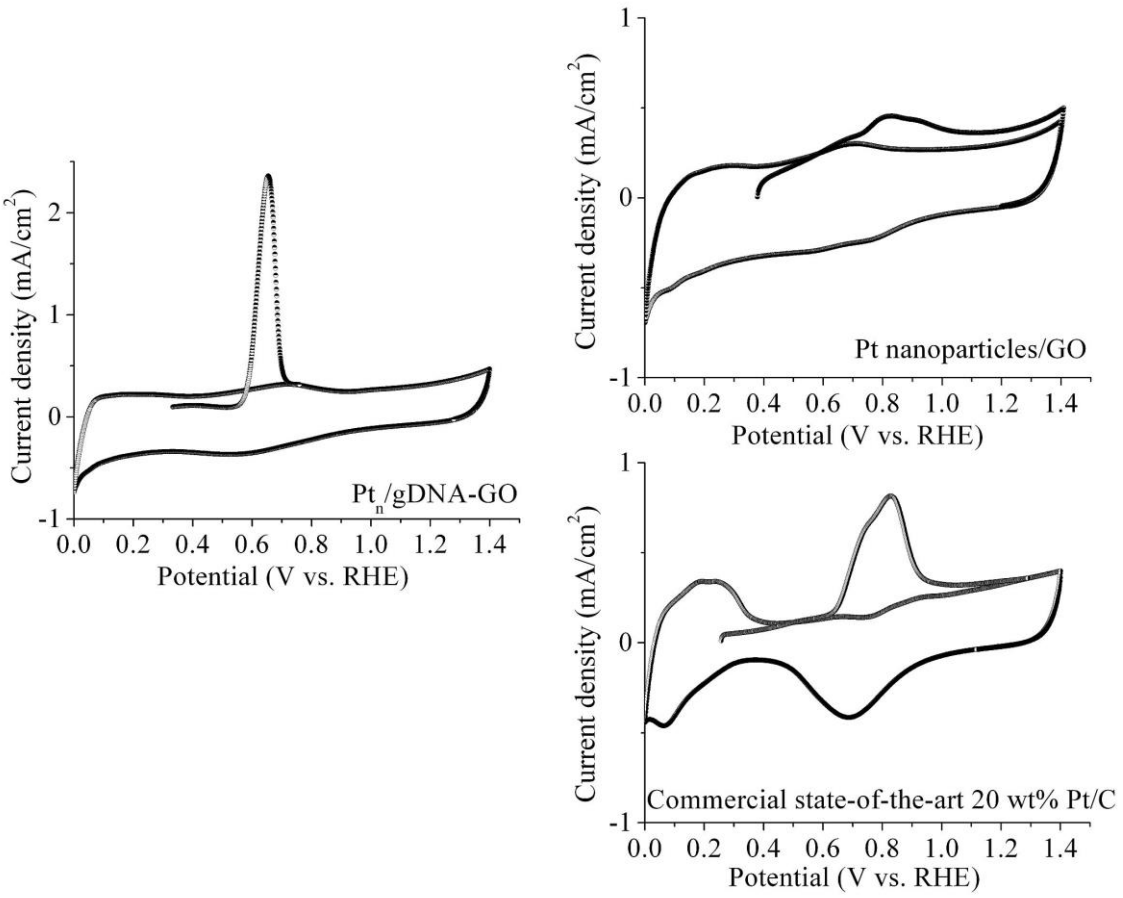

Supplementary Figure S15: CO stripping CV scan. CO stripping CV curves recorded at room temperature in 0.1 $HClO_4$ in the potential range 0 to 1.4 V vs. RHE with a scan rate of 20 mV/s for Pt_n/gDNA–GO, Pt nanoparticles/GO and Pt/C. The metal loading on the rotating-disk electrode was ~11.3 µg/cm^2 for Pt_n/gDNA–GO, Pt nanoparticles/GO and Pt/C.

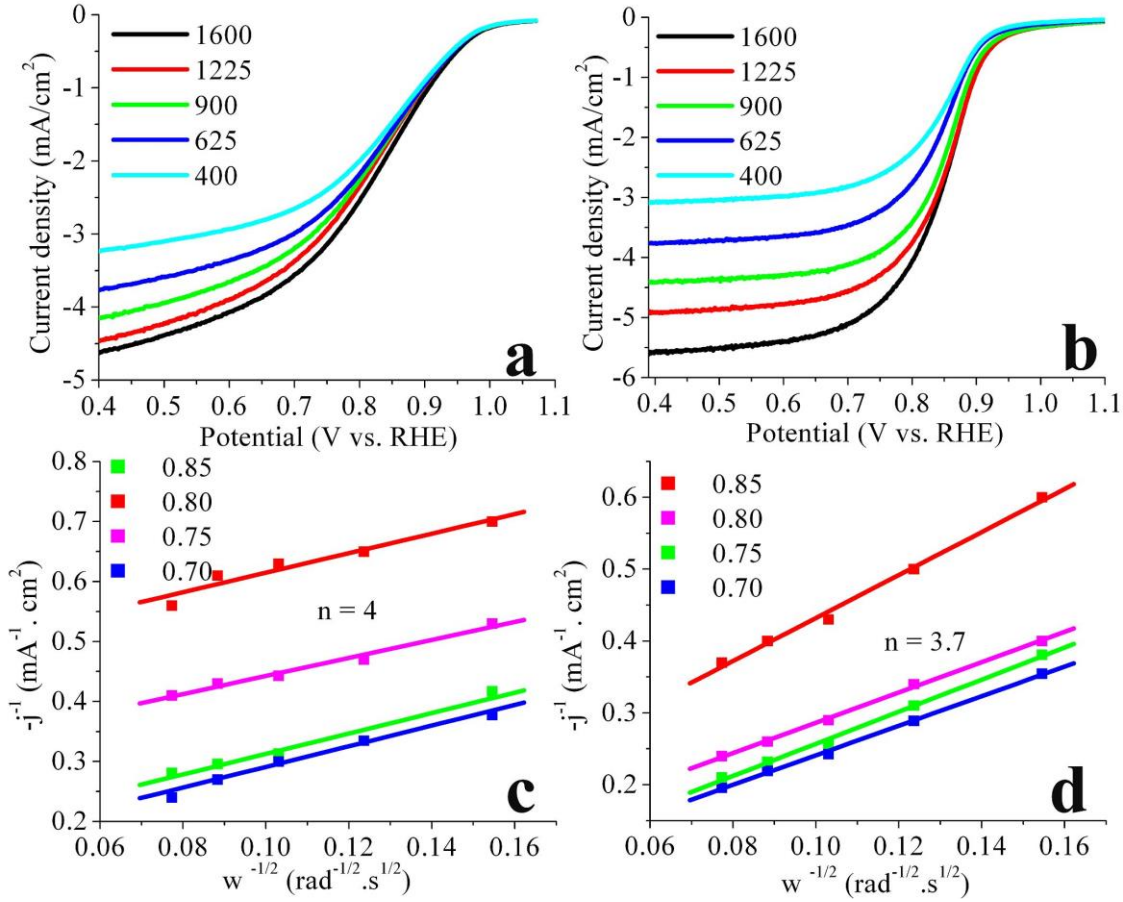

Supplementary Figure S16: ORR polarization curves and K-L plots. (**a**) and (**b**) ORR polarization curves of Pt nanoparticles/GO and Pt/C in O_2–saturated 0.1 M $HClO_4$ solution with a sweep rate of 10 mV/s at the different rotation speeds. (**c**) and (**d**) Corresponding K-L plots at various disk potentials. The linearity of j^{-1} vs. $w^{-1/2}$ displays a first order reaction with respect to dissolved oxygen in the electrolyte. The metal loading was ~11.3 µg/cm^2 on the rotating-disk electrode for the Pt nanoparticles/GO and Pt/C. In (a) and (b) current density was normalized in reference to the geometric area of a rotating-disk electrode (0.0707 cm^2).

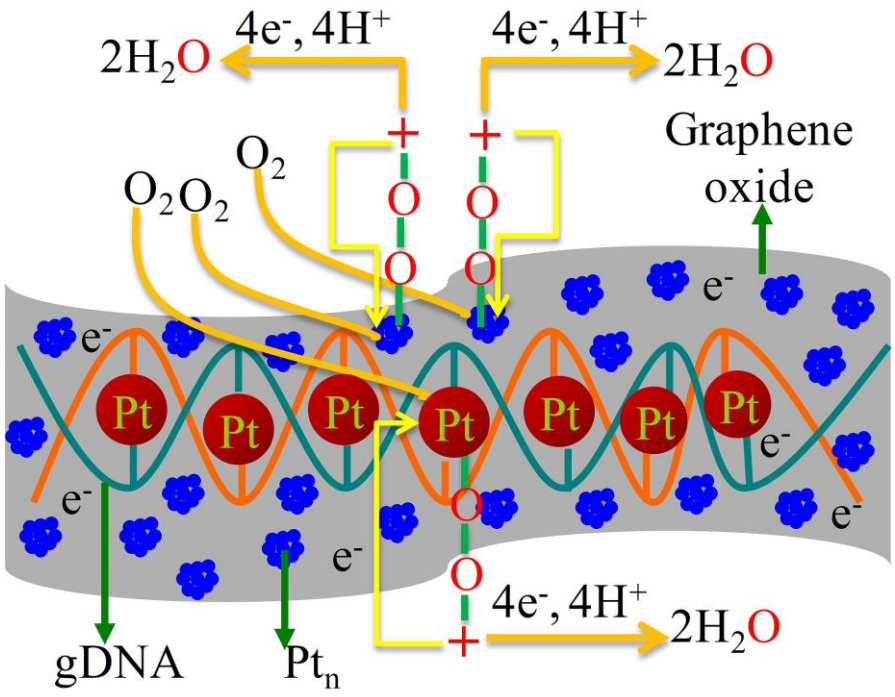

Supplementary Figure S17: ORR proposed mechanism. Schematic representation of the proposed mechanism involved in the ORR on the surface of Pt_n/gDNA–GO composite. The molecular oxygen is adsorbed and catalytically converted into atomic oxygen by the Pt_n and Pt nanoparticles. The atomic oxygen combines with $4e^-$ and 4 H^+ to form a water molecule. The H^+ and e^- are fed into the system from the electrolyte and external circuit, respectively.

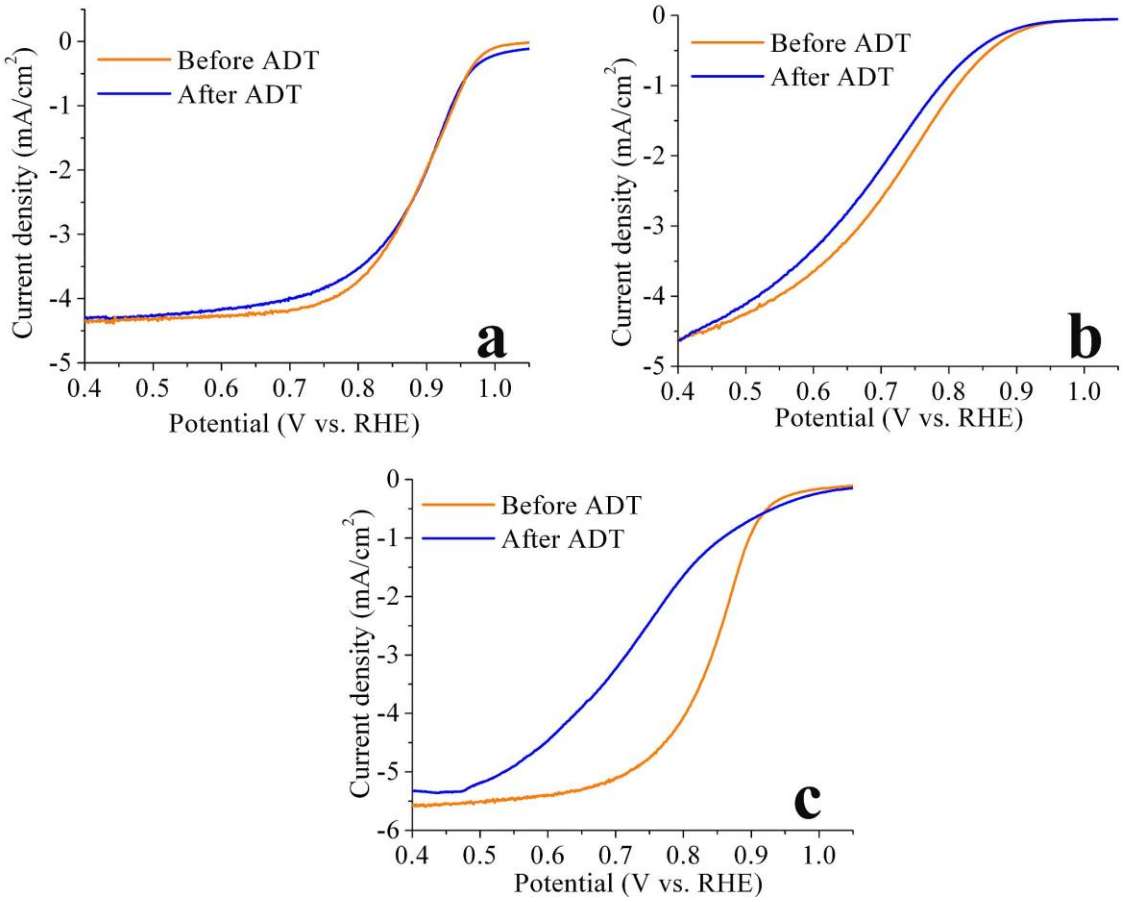

Supplementary Figure S18: ORR polarization curves before and after the ADT. Polarization curves of (a) Pt_n/gDNA–GO and (b) Pt nanoparticles/GO with comparison of Pt/C (c), before (orange color) and after (blue color) the ADT. This test was carried out in O_2–saturated 0.1 M $HClO_4$ with a scan rate of 10 mV/s at a rotation speed of 1600 rpm. The metal loading was ~11.3 µg/cm^2 on the GCE for the Pt_n/gDNA–GO, Pt nanoparticles/GO and Pt/C.

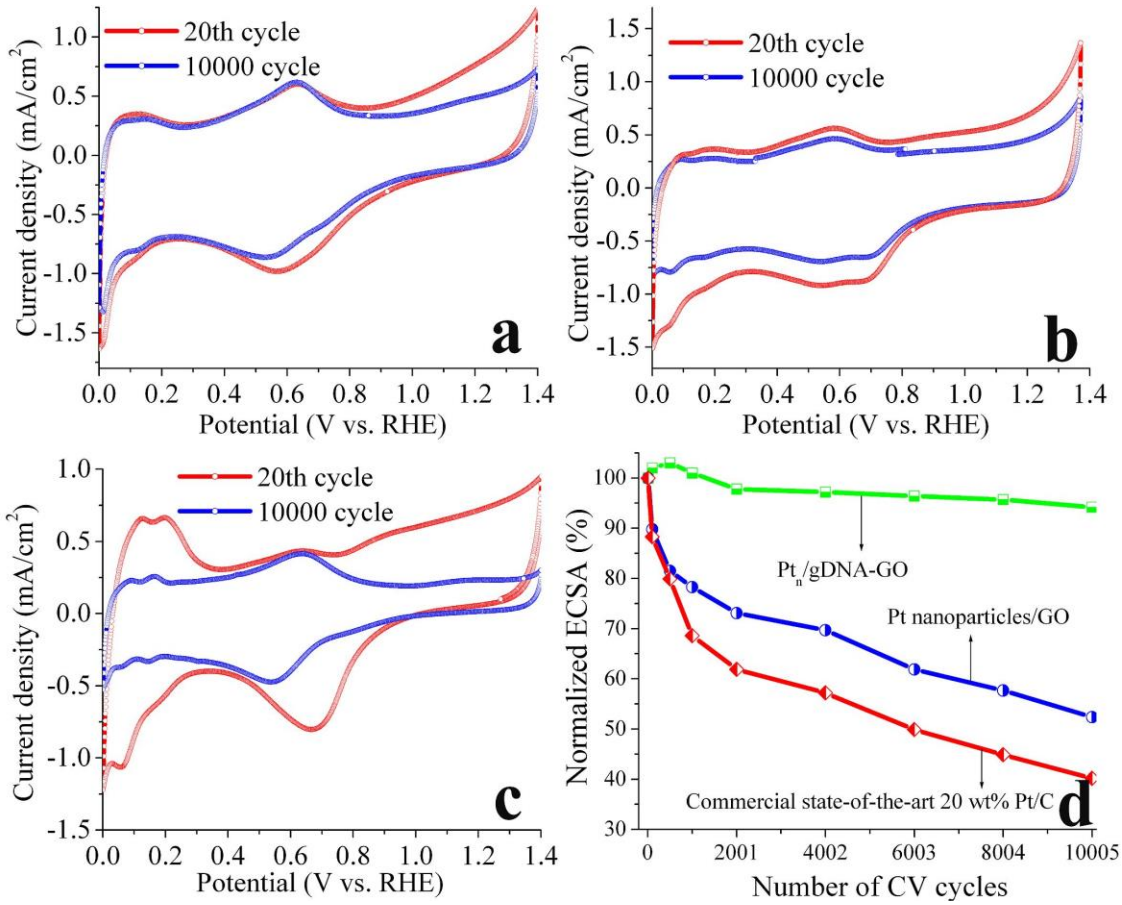

Supplementary Figure S19: CV stability test. CV curves of the 20 and 10000 cycles for (a) Pt_n/gDNA–GO, (b) Pt nanoparticles/GO and (c) Pt/C. (d) Loss of EASA for the three catalysts as a function of number of cycles in a N_2 saturated 0.1 M $HClO_4$ solution at room temperature (0.0–1.4 V vs. RHE, scan rate 50 mV/s). CV curves were used to determine the Pt surface area of the electrodes by measuring H adsorption before and after potential cycling. The H adsorption was calculated by integrating the charge between 0 and 0.37 V.

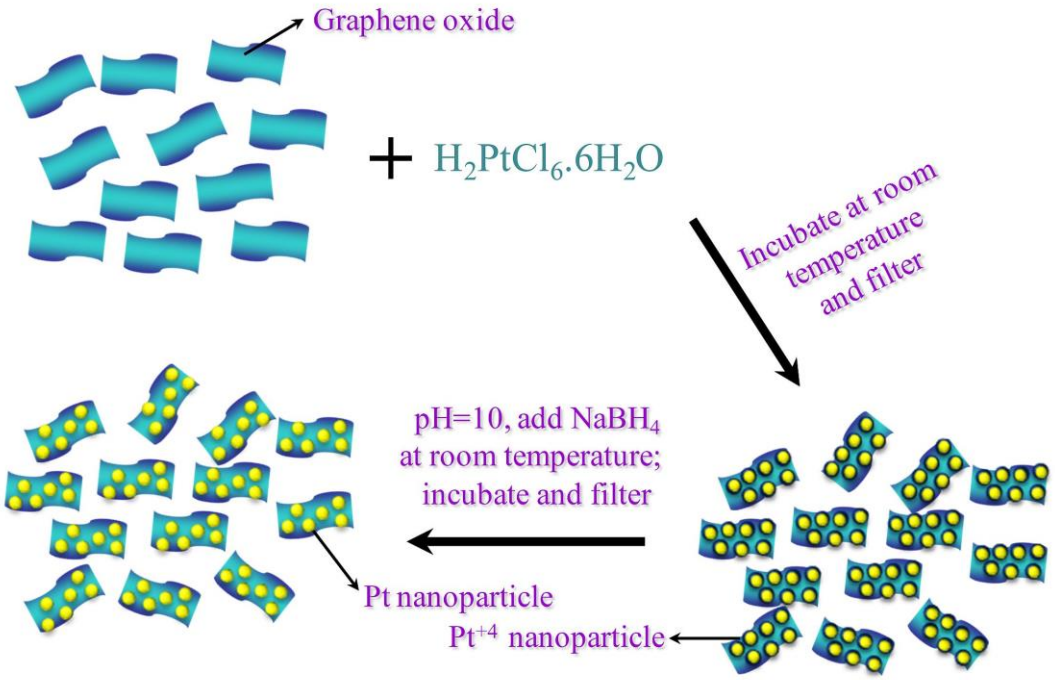

Supplementary Figure S20: Synthesis procedure. Schematic of the procedure used to prepare the Pt nanoparticles/GO composite.

Supplementary Table S1: Quantitative Analysis of the Pt_n/gDNA–GO composite using EDX. Fitting Coefficient: 0.8331

Element	(keV)	Mass%	Counts	Error%	Atom%	K
C K (Ref.)	0.277	66.72	384.18	0.01	86.08	1.0000
N K	0.392	10.82	104.82	0.05	11.98	0.5946
O K	0.525	0.19	2.52	1.53	0.18	0.4239
Pt M	2.048	22.27	144.34	0.07	1.77	0.8886
Total		100.00			100.00	

Supplementary Table S2: Quantitative Analysis of the Pt nanoparticles/GO using EDX. Fitting Coefficient: 0.9936

Element	(keV)	Mass%	Counts	Error%	Atom%	K
C K* (Ref.)	0.277	85.90	254.30	0.02	95.51	1.0000
N K*	0.392	0.74	3.69	3.03	0.71	0.5946
O K*	0.525	3.75	26.19	0.33	3.13	0.4239
Pt M*	2.048	9.61	32.03	0.68	0.66	0.8886
Total		100.00			100.00	

Supplementary Table S3: Comparison of the mass activities of other high performance Pt based ORR catalysts at 0.9 V vs. reversible hydrogen electrode.

Catalyst	Electrolyte	Scan rate (mVs^{-1})	Mass activity at 0.9V ($mA.\mu g^{-1}$)	Reference
Pd-Pt dendrites	0.1 M $HClO_4$	10	~0.204	32
Pt black	0.1 M $HClO_4$	10	~0.048	32
Starlike PtNW/C	0.1 M $HClO_4$	10	~0.135	66
Pt dendrites on C	0.1 M $HClO_4$	10	~0.045	67
Mesoporous double gyroid Pt	0.1 M $HClO_4$	5	~0.170	68
Au/Pt catalyst	0.1 M $HClO_4$	10	~0.223	69
Pt/RGO/CB-1	0.1 M $HClO_4$	10	~0.160	70
Pt_n/gDNA–GO	0.1 M $HClO_4$	10	~0.317	This work

Supplementary Methods

FTIR spectroscopy analysis

The synthesized products; GO, gDNA–GO, Pt nanoparticles/GO, and Pt_n/gDNA–GO samples were characterized by means of FTIR spectroscopy (Supplementary Fig. S2). In all samples, a broad absorption peak ranging from 3600 to 3000 cm^{-1} was observed which corresponds to the stretching of O–H bonds. In the GO sample, the characteristic absorption peaks at 1730, 1226, 1055 and 1620 cm^{-1} correspond to the stretching of C=O, C–OH, C–O and C=C/O-H bonds, respectively[48]. For the gDNA–GO composite the absorption bands at 1730, 1226 and 1055 cm^{-1} disappear and a single absorption peak at 1632 cm^{-1} is observed. Similarly, for the Pt nanoparticles/GO, only absorption peaks at 1637 cm^{-1} are observed. FTIR spectra observed for the composites (gDNA–GO and Pt nanoparticles/GO,) indicate the successful reduction of the GO using $NaBH_4$. The FTIR spectra of the Pt_n/gDNA–GO composite, shows two bands centered at 1090 and 1222 cm^{-1}, respectively, which can be attributed to the symmetric and anti-symmetric stretching vibrations of the phosphate group, while the peak at 1408 cm^{-1} can be assigned to the deformation peak of the O–H groups [49,50]. The band at 1566 cm^{-1} correspondeds to the C=C skeletal vibration of graphene sheets, which shows the GO sheets were successfully reduced using $NaBH_4$.

UV–vis Analysis

UV–vis spectroscopy confirms the successful synthesis of gDNA and GO, as well as gDNA–GO, (Supplementary Fig. S4). The UV-vis spectrum of GO exhibits two characteristic adsorption peaks, at 230 nm and 303 nm corresponding to the $\pi \rightarrow \pi^*$ transitions of aromatic C–C bonds and the $n \rightarrow \pi^*$ transitions of C=O bonds, respectively[51,52]. The peak at 230 nm was red shifted to ~254 nm upon chemical reduction, which suggests restoration of the electronic conjugation within the GO sheets (Supplementary Fig. S4)[53]. The characteristic adsorption peak of gDNA observed at ~256 nm is in agreement with previous reports[54]. In the case of gDNA–GO composites, the absorption peak appearing at ~260 nm is red shifted indicating that the gDNA firmly attaches to the surface of the GO sheets.

XPS and EDX analysis

The elemental composition and chemical bonding of the gDNA–GO, Pt nanoparticles/GO, and Pt_n/gDNA–GO samples were analyzed using XPS. The XPS spectrum of the gDNA–GO composite shows a strong P 2s peak at 190 eV, which correspond to the phosphate backbone of gDNA (Supplementary Fig. S8a)[55]. The gDNA–GO spectrum also shows a C 1s core level peak at 284.6 eV (Supplementary Fig. S8b), a N 1s core level peak at ~399.1 eV (amide, amine, aromatic nitrogen, Supplementary Fig. S8c), and an O 1s peak at 531.7 eV (Supplementary Fig. S8d). The existence of the amide bond is evidence of the binding on the gDNA to the GO sheet, while the existence of the P and N peaks is strong evidence for the inclusion of the gDNA into the composite material. In the gDNA-GO sample the C 1s core level XPS spectra shows the presence of C-C, C=C, C-N and C-OH groups, while the two peaks (284.6 and 286.7 eV) observed in the C 1s spectrum of GO (Supplementary Fig. S9) show the existence of C-C, C=C, C=O, COOH and C-O[56]. In the full survey XPS spectrum of the Pt nanoparticles/GO (Supplementary Fig. S10a) shows the existence of carbon, oxygen, platinum and nitrogen. The silicon peak observed in the sample was due to the use of a silicon wafer as a substrate material. Supplementary Figs. S10b-d shows the core level spectra XPS spectra for the Pt 4f, C 1s and N 1s core levels. The core level Pt 4f XPS spectrum (Supplementary Fig. S10b) can be deconvoluted into four peaks with binding energies centered at 71.4, 74.7, 72.6 and 76.1 eV. The peaks centered at 71.4 (4f7/2) and 74.7 eV (4f5/2) are attributed to zero-valent metallic Pt, while the peaks at 72.6, and 76.1eV are ascribed to PtO and PtO_2 species, respectively[57,58]. The C 1s core level peak (Supplementary Fig. S10c) is deconvoluted into two peaks with binding energies of 284.6 and 286.6 eV, corresponding to the C=C/C–C, and C-OH bonds, respectively. The XPS N 1s spectrum (Supplementary Fig. S8d) corresponds to the C=N bond with a binding energy of 400.5 eV, which is associated with the C=N bond[59]. Supplementary Fig. S11a shows the full survey XPS spectrum of the Pt_n/gDNA–GO composite, with clearly defined Pt 4f, Pt 4d, C 1s, P 2s, N 1s and O 1s core-levels. As in the gDNA-GO spectra, the Si peaks are attributed to the analysis substrate. To gain insight into the surface composition of the Pt_n/gDNA–GO composites, we conducted an HRXPS analysis for the Pt 4f, N 1s and C 1s core levels. The HRXPS spectra of the Pt 4f, C 1s and N 1s core

levels are shown in Supplementary Figs. S11b-d, respectively. The XPS Pt4f spectrum can be deconvoluted into two peaks with the binding energies located at 71.4 and 74.7 eV (Supplementary Fig. S11b) which are assigned to Pt 4f $_{7/2}$ and Pt 4f $_{5/2}$, respectively[60]. The C 1s core level spectrum (Supplementary Fig. S11c) can be deconvoluted into five components with binding energies centered at 283.7, 284.6, 285.6, 286.6 and 287.4 eV, attributed to the C-C, C=C, C-N, C-O and C=O groups, respectively. The XPS N 1s spectrum can be deconvoluted into two peaks with binding energies of 399.6 and 400.8 eV (Supplementary Fig. S11d), which can be attributed to amide, amine, aromatic nitrogen groups and quaternary N. The HRXPS N 1s core level XPS spectrum is similar to that observed for the gDNA–GO composite (Supplementary Fig. S8c), however an increased N content in the Pt_n/gDNA–GO composites is observed due to the incorporation of gDNA. The chemical compositions of the Pt_n/gDNA–GO and Pt nanoparticles/GO composites were further characterized by energy dispersive X–ray (EDX) spectra. The Pt_n/gDNA–GO composites and Pt nanoparticels/GO are composed mainly of carbon, oxygen, nitrogen and Pt atoms (Supplementary Figs. S12, S13, Supplementary tables S1 and S2), which is in agreement with the XPS data.

Isolation of genomic double stranded deoxyribonucleic acid (gDNA)

Pure genomic double stranded DNA (gDNA) was isolated from fully expanded mature leaves of *Arabidopsis thaliana* (*A. thaliana)* using the CTAB method[61,62] with some modifications. Briefly, *A. thaliana* plants were grown under controlled culture conditions at 22±2^{o}C with 60% relative humidity with a 16/8 h photoperiod. Approximately 75 g of the leaf tissue was ground to a fine powder in liquid nitrogen and suspended in CTAB buffer (2% Cetyl trimethylammonium bromide buffer (CTAB); 100 mM Tris buffer (pH 8); 20 mM Ethylene diamine tetraacetic acid (EDTA); 1.4 M Sodium Chloride (NaCl); 4% Polyvinylpyrrolidone (PVP, M_r=8000 gmol^{-1}) and 5 mM Sodium ascorbate) in a ratio of 1:3 (w/v). To eliminate RNA contamination, 100 µl of RNase (10 mg/ml) was added and the mixture was incubated at 65 ^{o}C for 10 min. To remove the protein contaminants the sample was treated with phenol:chloroform in a ratio of 1:1 (v/v) and centrifuged at 12000 rpm at room temperature for 10 min. The obtained supernatant was treated twice with an equal volume of chloroform:isoamylalcohol (24:1, v/v) followed by

centrifugation at 12000 rpm, 10 min at room temperature to remove all phenol traces. The gDNA was precipitated with 1/10 volume of isopropanol and washed twice with high grade 80% ethanol to remove any salt traces. The white pellet of gDNA was dried in a clean bench and then dissolved in 2 ml sterile triple distilled water. The sample was sonicated using an ULTRASONIC PROCESSOR, SONICS, Vibra Cell^{TM} (SONICS and MATERIALS Inc., CT, USA) at an amplitude control of 60% while being pulsed for 20 cycles at 10 sec intervals to create uniform size fragments of gDNA of about 300–700 base pairs. The gDNA was then purified again and resuspended to a final concentration of 6 mg/mL, quantified using an Infinite® 200 NanoQuant (Mannedorf, Switzerland). The quality of the gDNA was determined by measuring its $A_{260/280}$ absorbance ratio, as well as electrophoresis (see Supplementary Fig. S1).

Preparation of graphene oxide

A detailed description of the synthesis process of graphene oxide (GO) has been reported elsewhere[63]. In a typical synthesis 2g of graphite powder was mixed with conc. H_2SO_4 (50 ml) and 2g $NaNO_3$ at 0°C. 6g (37.967 mmol) of $KMnO_4$ was slowly added to the flask while maintaining vigorous stirring and the temperature was kept below than 15°C. The mixture was stirred at 35°C until it became pasty brownish, and it was then diluted using de-ionized (DI) water. 10 ml H_2O_2 (30 wt. %) solution was slowly poured into the mixture, after which the color of the mixture changed to bright yellow. The mixture was centrifuged, wherafter the pellet was resuspended and washed with a 1:10 HCl aqueous solution in order to remove residual metal ions. The resulting precipitate was washed repeatedly with DI water until a neutral pH was observed. The GO used in the synthesis was obtained by drying the precipitate in a vacuum.

Sample preparation for physicochemical characterization

Raman and X-ray photoelectron spectroscopy (XPS) samples were prepared by coating a thin film of the sample on a silica wafer at room temperature. Fourier transform infrared (FTIR) samples were prepared by mixing a small amount of sample with potassium bromide powder, which is transparent to the incident IR radiation, and pressing into pellets in a die. Ultraviolet–visible (UV-vis) samples were prepared by dissolving gDNA, GO and gDNA–GO in DI water.

Electrochemical measurements

Electrochemical measurements were performed using a glassy carbon rotating-disk electrode (Bio-Logic Science Instruments) connected to a VSP-Modular 2 Channels Potentiostat/Galvanostat/EIS. A typical three-electrode configuration was employed, consisting of a modified glassy carbon electrode (3 mm in diameter) as the working electrode, Ag/AgCl (3 M NaCl) reference electrode and platinum wire as a counter electrode in 0.1 M $HClO_4$. All potentials were converted to values with reference to a reversible hydrogen electrode. To perform the RHE conversion, the thermodynamic potential for the hydrogen electrode was needed. This potential was obtained using cyclic voltammetry. From cyclic sweeps at a sweep rate of 1 mV/s, the average of the two potentials at which the current crossed zero was taken to be the thermodynamic potential for the hydrogen electrode reaction.

Preparation of working electrodes

1 mg of catalyst was dispersed in a 1 ml DI water using sonication. 4μl of the dispersed sample solutions were then transferred onto the glassy carbon rotating-disk electrode with a geometric area of 0.0707 cm^2. After evaporation of the water, the electrode was covered with 4 μl of 0.05 wt% Nafion solution. Finally, the electrodes were put in a vacuum oven for two days at 80 °C before measurement.

Loading amount of Pt is calculated by following method:

Concentration of catalysts x loading of catalysts on RDE x wt% of catalysts

In our case: 1mg x 4 μl x 20/100 x 1000 μl = 0.0008 mg

In respect of area, the amount of Pt = 0.0008/0.0707 = 0.011315 mg/cm^2 = 11.31 μg/cm^2

CV measurements

Cyclic voltammetry (CV) measurements were carried out under nitrogen in 0.1 M $HClO_4$ aqueous solution at a scan rate of 50 mVs^{-1}. CV plots were used to determine the electrochemically active surface area (EASA) of the electrodes by measuring the charge associated with under-potentially deposited hydrogen (H_{upd}) adsorption between 0 and

0.37 V, assuming 0.21 mC/cm^2 for deposition of a H monolayer on a Pt surface. The H_{upd} adsorption charge (Q_H) can be easily calculated using the following equation[64]:

$$Q_H[C] = \int_{0.0}^{0.37} \frac{I\,[A] \times dE[V]}{v[V/s]} \qquad (S1)$$

where C is charge, I the current, E the potential, v the scan rate, and Q the charge in the Hupd adsorption/desorption area obtained after double-layer correction. Then, the specific EASA was calculated based on the following equation[64]:

$$\text{Specific EASA} = Q_H / m \times q_H \qquad (S2)$$

where Q_H is the charge for Hupd adsorption, m is the loading amount of metal, and q_H is the charge required for monolayer adsorption of hydrogen on a Pt surface.

CO-stripping cyclic voltammetry

The background electrochemical measurement was performed in a N_2-saturated 0.1 M $HClO_4$ electrolyte solution over the potential range 0 to 1.4 V (vs. RHE) at a scan rate of 20 mV/s. The CO adsorption on the Pt catalyst was performed by bubbling a 10% CO/N_2 gas mixture into the 0.1 M $HClO_4$ electrolyte solution at a constant potential of 0.1 V (vs. RHE) for 2000 s. The EASA was calculated from the integrated charge (after background correction) under the CO oxidation peak of the first scan obtained from the CO stripping measurement using the following equation:

$$\text{ESA} = Q_{CO}/\{Pt\} \times 0.420 \qquad (S3)$$

$$Q_{CO} = \int i\, dE/2\upsilon \qquad (S4)$$

where Q_{CO} is the CO stripping charge (mC), [Pt] is the mass loading per unit area of the Pt catalyst, 0.420 mC/cm^2 corresponds to a monolayer of adsorbed CO and υ is the scan rate.

Calculation of electron-transfer rate, mass and specific activities

For the rotating-disk electrode experiments, all sample solutions were prepared by the same method as CV's. 4 μl solution (containing 1 mg/1mL catalyst) was loaded on a glassy carbon rotating disk electrode of 3 mm in diameter. The working electrode was scanned cathodically at a sweep rate of 10 mVs^{-1} with different rotating-disk electrode rotation rates: 400, 625, 900, 1225, and 1600 rpm. Koutecky–Levich (K-L) curves (J^{-1} vs.

$w^{-1/2}$) for the catalyst samples were analyzed at different potentials (Fig. 3b, Supplementary Figs. S16c, d). The slopes of their best linear fit lines were used to evaluate the number of electrons transferred (n) on the basis of the K-L equation:

$$1/j = 1/j_k + 1/j_d = 1/j_k + 1/Bw^{1/2} \quad \text{(S5)}$$

in which

$$B = 0.62nFAC_{O_2}D_{O_2}^{2/3}/\eta^{1/6} \quad \text{(S6)}$$

where j is the experimentally obtained current, j_k is the kinetic current, j_d is the diffusion- limiting current, n is the number of electrons transferred, F is Faraday's constant (F = 96485.34 C/mol), A is the electrode's geometric area (A = 0.0707 cm^2), C_{O_2} is the O_2 concentration in the electrolyte (C_{O_2}=1.26 x 10^{-3} mol/L), D_{O_2} is the diffusion coefficient of O_2 in the $HClO_4$ solution (D_{O_2} = 1.93 × 10^{-5} cm^2/s), and η is the viscosity of the electrolyte (η = 1.009 × 10^{-2} cm^2/s) [65].

From supplementary eq. S5, the kinetic current was calculated based on the following equation[39]:

$$J_k = (j \times j_d)/(j_d - j) \quad \text{(S7)}$$

For each sample, the kinetic current was normalized to loading amount of metal and EASA to obtain mass and specific activities, respectively.

Supplementary References

48. Zhou, M., Zhai, Y. M. & Dong, S. J. Electrochemical sensing and biosensing platform based on chemically reduced graphene oxide. *Anal. Chem.* **81**, 5603–5613 (2009).

49. Yamada, M. & Amoo, M. Enzymatic collapse of artificial polymer composite material containing double-stranded DNA. *Int. J. Biol. Macromol.* **42**, 478–482 (2008).

50. Zhang, H., et al. Microwave-assisted synthesis of graphene-supported Pd_1Pt_3 nanostructures and their electrocatalytic activity for methanol oxidation. *Electrochim. Acta* **56**, 7064–7070 (2011).

51. Paredes, J. I., Villar-Rodil, S., Martínez-Alonso, A. & Tascón, J. M. D. Graphene oxide dispersions in organic solvents. *Langmuir* **24**, 10560–10564 (2008).

52. Li, J. & Liu, C.-Y. Ag/graphene heterostructures: synthesis, characterization and optical properties. *Eur. J. Inorg. Chem.* **2010**, 1244–1248 (2010).

53. Li, D., Muller, M. B., Gilje, S., Kaner, R.B. & Wallace, G. G. Processable aqueous dispersions of graphene nanosheets. *Nat. Nanotechnol.* **3**, 101–105 (2008).

54. Liu, L., Li, Y., Li, Y., Li, J. & Deng, Z. Noncovalent DNA decorations of graphene oxide and reduced graphene oxide toward water-soluble metal–carbon hybrid nanostructures via self-assembly. *J. Mater. Chem.* **20**, 900–906 (2010).

55. Bae, A. H., Hatano, T., Numata, M., Takeuchi, M. & Shinkai, S. Superstructural poly(pyrrole) assemblies created by a DNA templating method. *Macromolecules* **38**, 1609–1615 (2005).

56. Fu, X., Wang, Y., Wu, N., Gui, L. & Tang, Y. Surface modification of small platinum nanoclusters with alkylamine and alkylthiol: an XPS study on the influence of organic ligands on the Pt 4f binding energies of small platinum nanoclusters. *J. Colloid Interface Sci.* **243**, 326-330 (2001).

57. Alderucci, V., et al. XPS study of surface oxidation of carbon-supported Pt catalysts. *Mater. Chem. Phys.* **41**, 9–14 (1995).

58. Hufner, S. & Wertheim, G. K. Core-line asymmetries in the x-ray-photoemission spectra of metals. *Phys. Rev. B* **11**, 678–683 (1975).

59. Zhao, L., Hu, Y.-S., Li, H., Wang, Z. & Chen, L. Porous $Li_4Ti_5O_{12}$ coated with N-doped carbon from ionic liquids for Li-ion batteries. *Adv. Mater.* **23**, 1385–1388 (2011).

60. Xin, Y., et al. Preparation and characterization of Pt supported on graphene with enhanced electrocatalytic activity in fuel cell. *J. Power Sources* 196, 1012-1018 (2011).

61. Kasajima, I. et al. A protocol for rapid DNA extraction from *Arabidopsis Thaliana* for PCR analysis. *Plant Mol. Biol. Rep.* **22**, 49–52 (2004).

62. Gupta, A. K., Harish Rai, M. K., Phulwaria, M. & Shekhawat, N. S. Isolation of genomic DNA sitable for community analysis from mature tree adapted to arid environment. Gene, (2011) July.

63. Tiwari, J.N., Mahesh, K., Le, N.H., Kemp, K.C., Timilsina, R., Tiwari, R.N. & Kim, K.S. Reduced graphene oxide-based hydrogels for the efficient capture of dye pollutants from aqueous solutions. *Carbon* **56**, 173–182 (2013).

64. Lee, E. P. et al. Growing Pt Nanowires as a Densely Packed Array on Metal Gauze. *J. Am. Chem. Soc.* **129**, 10634–10635 (2007).

65. Kim, D. S., Zeid, E. F. A. & Kim, Y. T. Additive treatment effect of TiO_2 as supports for Pt-based electrocatalysts on oxygen reduction reaction activity. *Electrochim. Acta* **55**, 3628–3633 (2010).

66. Sun, S. et al. A highly durable platinum nanocatalyst for proton exchange membrane fuel cells: multiarmed starlike nanowire single crystal. *Angew. Chem. Int. Ed.* **50**, 422–426 (2011).

67. Kim, C., Oh, J. G., Kim, Y. T., Kim, H. & Lee, H. Platinum dendrites with controlled sizes for oxygen reduction reaction. *Electrochem. Commun.* **12**, 1596–1599 (2010).

68. Kibsgaard, J., Gorlin, Y., Chen, Z. & Jaramillo, T. F. Meso-structured platinum thin films: active and stable electrocatalysts for the oxygen reduction reaction. *J. Am. Chem. Soc.* **134**, 7758−7765 (2012).

69. Tan, Y., Fan, J., Chen, G., Zheng, N. & Xie, Q. Au/Pt and Au/Pt_3Ni nanowires as self-supported electrocatalysts with high activity and durability for oxygen reduction. *Chem. Commun.* **47**, 11624–11626 (2011).

70. Li, Y. et al. Stabilization of high-performance oxygen reduction reaction Pt electrocatalyst supported on reduced graphene oxide/carbon black composite. *J. Am. Chem. Soc.* **134**, 12326–12329 (2012).